TECHNISCHE MECHANIK, 32, 2-5, (2012), 577 – 586
submitted: November 1, 2011

Characterization of High Carbon Steel C68 at Elevated Temperatures and Different Strain Rates

M. Vautrot, P. Balland, O.S. Hopperstad, L. Tabourot, J. Raujol-Veille, F. Toussaint

This paper presents high-temperature tensile testing. This method is used to characterize the mechanical behaviour of a high-carbon steel C68 at temperatures up to 720°C. Samples are heated by an induction system controlled with a pyrometer. A high-speed camera (500 fps) is used to determine the displacement field with a digital image correlation software. For such tests a specific marking procedure of the sample is applied. Stress-strain curves are given from room temperature up to 720°C at strain rates ranging from $10^{-3}\ /s$ *to* $10^{-1}\ /s$*. Elastic parameters of the material are measured at room temperature using cyclic tests. Bridgman's method is used to determine the equivalent stress-plastic strain curve during the necking phase.*

Introduction

In the field of metal forming, extreme conditions are nowadays imposed to materials in order to always produce more precise parts with more added value at lower cost. Under such conditions, a numerical simulation appears now as one of the best solutions to check the feasibility of the forming operation when compared with some costly, time-consuming, trial and error empirical methods. The finite element method requires elaborate constitutive equations describing the mechanical behavior (namely a stress-strain relationship) as realistic as possible. As general modeling approaches that could describe the mechanical behavior for any material under any loading conditions do not exist yet, each process and material combination requires a dedicated modeling strategy. Indeed, any phenomenological model has strong limitations: it is basically capable of giving back experimental evidence corresponding to those used in the experimental identification. Consequently, it is crucial that the experimental characterization makes use of loading conditions corresponding to those imposed by the processing of the material if one wants to succeed in the simulation of the forming process. Respecting these preliminary conditions, the experimental protocol should assure the best determination of the stress-strain relation for a given representative elementary volume. The case study is here an incremental forming process (Raujol-Veillé et al., 2011) applied to C68 steel sheets in order to obtain industrial components with accurate geometry. An induction device is used to heat the workpiece before forming. Such process imposes strain rates ranging for 0 to $10^2\ /s$ for productivity reason and temperatures up to 720°C (just below phase transition temperature) to obtain good ductility and avoid fracture of the material during forming. Formed parts are subjected to considerable springback during unloading, giving the elastic parameters an important role.

Within this industrial framework, the material characterization should be in accordance with the following specifications:

- testing should impose the same thermo-mechanical conditions as those imposed by the process,
- the quality of the results of the mechanical characterization of materials should be obtained at reasonable delay and good financial cost from an industrial point of view.

Therefore one needs to build an experimental database that gives stress-strain curves in the elastic and plastic domains for various temperatures and for a range of strain rates corresponding to those imposed by the process. The objective of this paper is to define and validate the experimental setup that will be used to characterize the C68 steel behavior under such conditions. Some preliminary results are given to show the efficiency of the proposed method.

After a brief presentation of the material in the first section, the second section describes the procedure for high-temperature tensile testing. Then, the third section presents some first experimental results for the elastic and plastic behaviour of the C68 material.

1 Material

The C68 steel is delivered in 1.54 mm thick sheets in an annealed state. Its chemical composition is reported in Table 1.

C	Mn	Si	P	S	P+S	Cr	Al
0.65-0.73	0.50-0.80	0.15-0.35	0-0.035	0-0.025	0-0.05	0.15-0.30	0.005-0.030

Table 1. C68 chemical composition (in weight %)

Even if the maximum temperature (720°C) is below the phase transition temperature, it should be checked that such heating does not affect the microstructure of the material. This would introduce physical effects that a usual phenomenological modeling could not consider. Therefore, the material is heated up to 720°C and micrographies of the delivered material and the material after heating are compared. Simultaneously, the microhardness of the material for both states is compared. Figure 1 and Table 2 show the microstructure and the microhardness of the material in the delivered state and after heating to 720°C using an induction system. The analysis of this microstructure allows us to highlight the globular aspect of the material characterizing a globular annealing in the delivered state. It is formed of cementite globulars in a ferritic matrix.

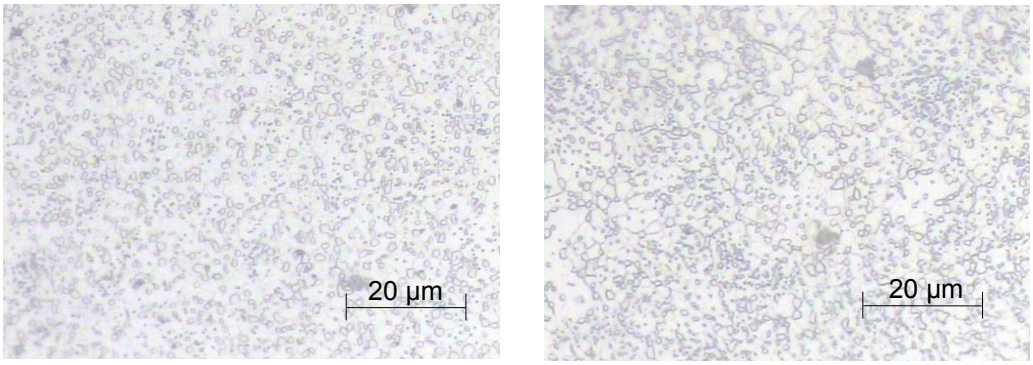

Figure 1. C68 microstructure in the delivered state (left) and after heating to 720°C using an induction system (right)

Material state	Microhardness (HV5)
Delivered state	200
After induction heating	200

Table 2. C68 microhardness in the delivered state and after heating TO 720°C using an induction system

These investigations do not reveal any effect of the heating on the microstructure and the microhardness of the material.

2 High-Temperature Tensile Testing

The first objective is to provide the means to get the behaviour at high-temperature with the necessary accuracy required by a finite element simulation. In spite of the fact that multi-axial testing should be used to account for the complex loading applied industrially to the material, in this paper, a monotonic uniaxial tensile test is used to concentrate only on the heating process and strain measurements at high-temperature. Measuring accurate true stress-strain curves at high-temperature is not an easy task and brings two main challenges:

- how to heat the sample and control the temperature?
- how to measure the strain field induced by a mechanical load at high-temperature?

To heat a sample at this temperature, several experimental devices can be employed like high-temperature furnace, ohmic heating or induction heating (Pan et al., 2010). Some furnaces are capable of heating up a sample to 720°C but with lower heating and cooling rates due to a large thermal inertia in the chamber. Moreover, digital image correlation (DIC) is penalized when using furnaces because of the quality of recorded digital images we want to obtain. The ohmic and the induction heating allow for rapid heating but with some difficulties to control temperature.

Both contact and non-contact techniques can be used to measure high-temperature strains. Commonly, high-temperature strains are measured by extensometers or strain gauges. But this technique can only give us the average strain in a local area. To obtain full-field strain measurements, a non-contact optical technique like DIC is necessary. Lyons et al. (1996) succeeded to determine the full-field strain using DIC at high-temperature up to 650°C for an Inconel 718 alloy. His method is used by Liu et al. (1998a,b) to characterize Alloy 800 and Alloy 718 at high-temperatures. Pan et al. (2010) devised an experimental set-up using the DIC technique to extract the full-field strain of metals and alloys at temperatures from room temperature up to 550°C. In this paper, tests are conducted at temperatures from room temperature to 720°C.

In order to obtain the accurate local strain, digital image correlation is used in combination with an induction system. The induction system is chosen for two reasons: (1) the sample is not enclosed in a chamber and it makes it easier to use a camera, and (2) it is used in the industrial process. Furthermore, a non-contact technique, like DIC, could allow us to develop, in the next stage, a heterogeneous test to account for complex loading conditions as explained above. An extensometer is not suitable for such tests. This section describes the experimental setup corresponding to these prescriptions.

2.1 Experimental Set-Up

The experimental set-up for the uniaxial tensile testing is shown in Figure 2. The tensile test machine is an INSTRON® 5569 model. A CEIA 6 kW induction system is used to heat the sample. The heating head is placed behind the specimen. The temperature control is done by a pyrometer IMPAC IPE 140 placed in front of the specimen. The temperature control of this equipment is ranging from 30-1000°C. The accuracy is between 2.5°C and 3.9°C in the studied range of temperatures. Table 3 shows the experimental accuracy (third column) and the theoretical accuracy from the documentation (fourth column) of the pyrometer IPE 140 at some temperatures measured for a black body with an emissivity of 0.99. The results show a good accuracy of the pyrometer in the targeted experimental temperature range.

Reference temperature (°C)	Temperature from IPE 140 (°C)	ΔT (°C)	Theoretical ΔT (°C)
70	72.7	2.7	2.5
150	150.3	0.3	2.5
260	257.4	2.6	2.5
500	497.4	2.6	3
781	780.7	0.3	4.1

Table 3. Experimental accuracy ΔT of the pyrometer for some representatives temperatures

Images for correlation are acquired by a CMOS EoSens CL high-speed camera (resolution 1280 x 1024 pixels) coupled with a 24-88 mm f/2.8-4 Nikon objective. This camera is capable of acquiring images up to 500 frames per second at full resolution and up to 120 000 frames in low resolution. This range is necessary to study a strain rates ranging from $10^{-3}\ /s$ to $10^{-1}\ /s$. The focal plane of the objective of the camera is roughly located at 450 mm from the surface of the sample.

To apply the DIC method at room temperature and at temperatures under 200°C, the samples are beforehand painted with white paint to avoid reflections of the surface on the video. Then, samples are speckled with black paint and primary colors. Figure 3 shows the grey levels on the surface of a sample of two speckles. The first speckle is only done with white and black paints, while for the second speckle primary colors are added. The addition of primary colors broadens the grey level spectrum registered by the camera, and allows to exploit grey levels ranging between 0 and 50 (Temimi-Maaref, 2006). A broadening grey level spectrum allows for a better post-processing with an image correlation software. Indeed, the more speckles are contrasted, the more easily the software is going to find the full strain field.

Between 200°C and 720°C, painted patterns are burning, so an other marking system is necessary. The electro-

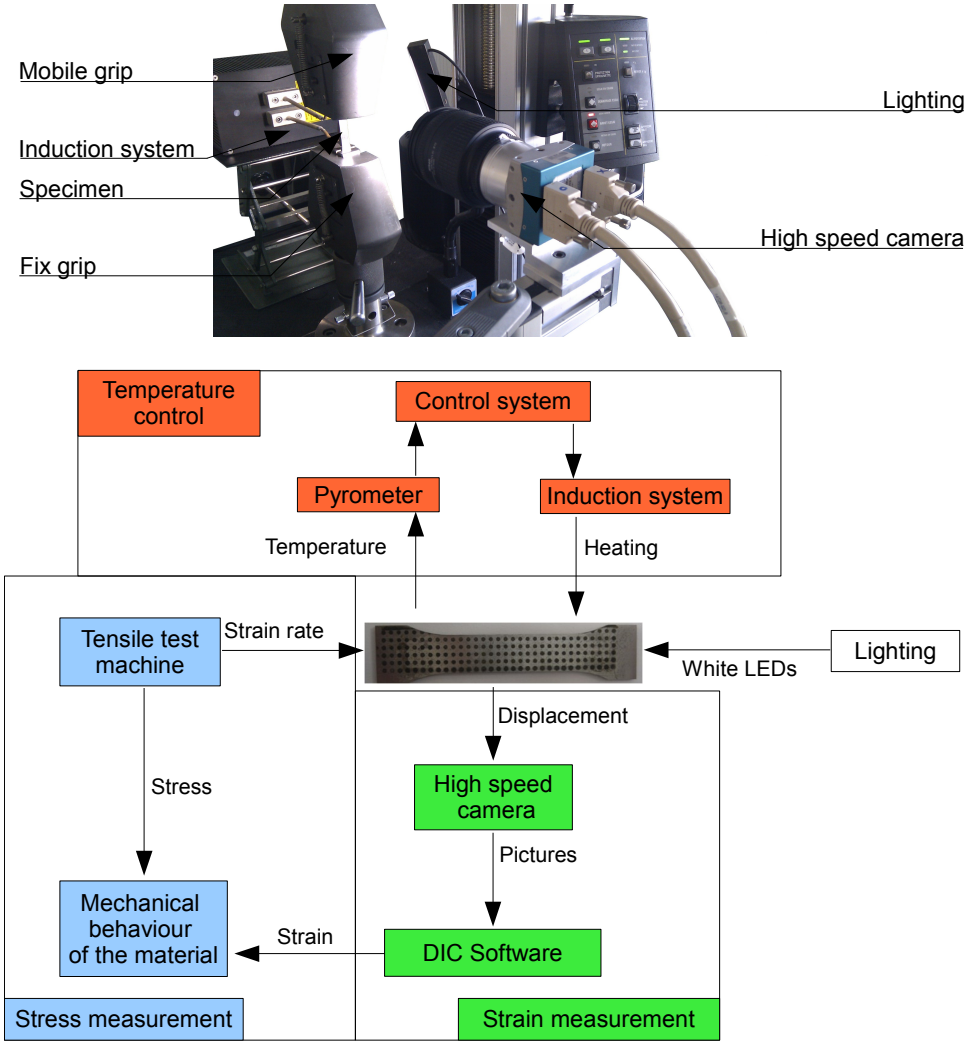

Figure 2. Experimental setup and synoptic of the experimental configuration in the case of uniaxial tensile tests

chemical marking ME3000S from Metaletch has been chosen to realize a pattern on the surface of the sample. With this system, an oxide film is created on the surface using a stencil and an electrochemical machine. The chosen pattern is a regular grid composed of 1 mm-diameter filled circles with 2 mm spacing as shown in Figure 4. In that case, the grey level spectrum is less homogeneous than in the first case with paints, but it is the only means to use DIC, which is still better than using the crosshead displacement.

To obtain usable images, homogeneous and stable lighting of the sample surface is required. Indeed, if a speckle receives light with a stronger intensity than another, DIC would be affected leading to inaccurate displacement determination. Even worse, under such conditions the software would sometimes be unable to process images. The lighting system is a bar of LEDs including 3 rows of 32 LEDs which diffuses white light with wavelength in the range 400-700 nm.

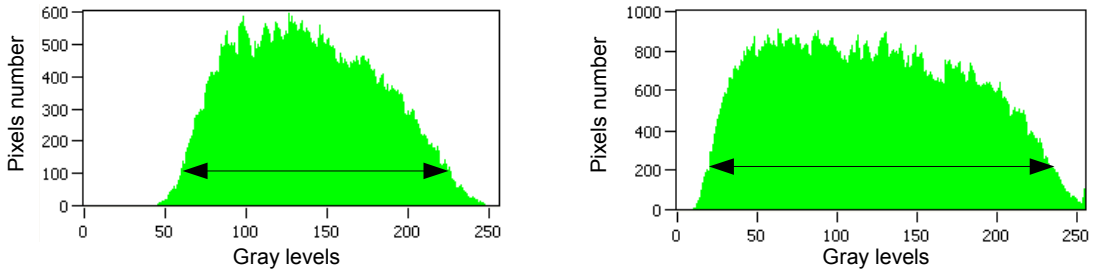

Figure 3. Grey level distribution histogram on the sample surface (levels from 0 to 255) of pixels of a black and white speckle (on the left) and with an addition of primary colors (on the right)

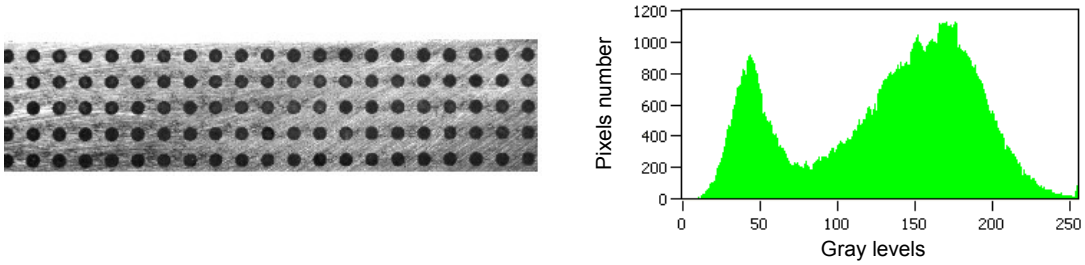

Figure 4. Pattern on the surface of the specimen (on the left) and grey level distribution histogram on the sample surface using electrochemical marking (on the right)

2.2 Determination of Strain and Stress

The used digital image correlation software, 7D, is developed by Vacher (Vacher et al., 1999). A rectangular area in the middle of the reference image, as shown in Figure 5, is chosen as the region of interest. This area corresponds to the area heated by the induction system. For each transverse section, major and minor strain values of each node of this grid are calculated and averaged.

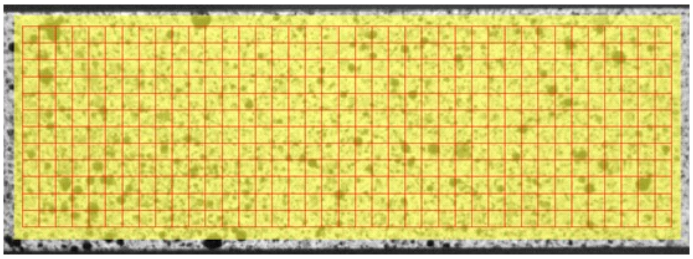

Figure 5. Virtual grid used by digital image correlation method

The incremental forming process in the case study imposes a maximum strain about 100 % (Raujol-Veillé et al., 2011). Therefore it is necessary to go as far as possible in the strain analysis. When respecting the homogeneous stress/strain hypothesis, the maximum strain obtainable with a tensile test on this material is about 20 % which corresponds to the onset of the diffuse necking. After this point, non-uniform deformation starts and ends at fracture. Just before fracture, for flat specimens, a local shear band is usually formed on the necked surface of the specimen. The appearance of the band charactizes the onset of localized necking. To go further in our analysis, a solution is to analyse data even when diffuse necking occurs.

The onset of diffuse necking begins at the point of maximum stress on the engineering stress-strain curve, when the internal force reaches a maximum value. The stress distribution in the necking area is not uniform anymore and becomes triaxial. The computation of true stresses should consider this non-uniform distribution. For a cylindrical tensile specimen, Bridgman (1952) proposed a method to estimate the stress evolution. However, Bridgman's estimation is not easy to apply in practice and requires the geometry evolution of the specimen in the necking area. To overcome this difficulty, Le Roy et al. (1981) have proposed a method to determine the specimen geometry in the necking area, supposing that the geometry of the cylindrical specimen can be approximated by a circle in the necking area, as shown in Figure 6. Flat specimens are used as frequently as cylindrical specimens, especially when studying sheet metals. Bridgman-Le Roy's estimation has been used and validated by Zhang et al. (1999) for flat specimens.

Due to transverse strains determined from the surface displacement obtained by DIC, the profile of the necked area can be rebuilt as shown in Figure 6. Afterwards, using Matlab, an automatic procedure detects the necking and its localisation. The radius is deduced from the profile of the necking area by fitting a circle.

Bridgman's estimation is applied as soon as the diffuse necking occurs, until the onset of localized necking which leads to ductile fracture. This method allows us to obtain a maximum strain after necking until 50 %.

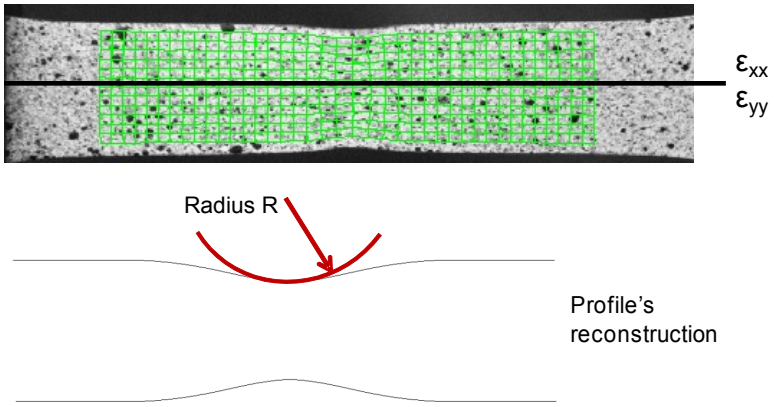

Figure 6. Profile reconstruction using transverse strains obtained by the DIC method

3 Elastic Behaviour

3.1 Determination of the Young's Modulus

In forming processes, the Young's modulus is a very important parameter when springback is occuring (Morestin and Boivin, 1996). Thus, an accurate evaluation of Young's modulus is essential. The evolution of Young's modulus with plastic strains is experimentally determined from samples pre-deformed to strains from 0 % to 15 %. All tests are performed at room temperature with a strain rate at $5.10^{-4}\ /s$ on the Instron tensile testing machine. For better accuracy in the elastic area, the strain is determined by an extensometer with gauge length 12.5 mm.

Young's modulus is determined by linear regression in the elastic area. The lower limit of the linear regression corresponds to 10 % of the yield stress to avoid the nonlinearity at the beginning of the test and the upper limit to 50 % of the yield stress to avoid microplasticity. The final Young's modulus is determined as the average of 50 measurements obtained for successive loading-unloading cycles. Table 3 shows the result of Young's modulus measurements according to previous parameters.

Material	Young's modulus (GPa)	Standard deviation (GPa)
C68	211	1.56

Table 3. Young's modulus for C68

3.2 Young's Modulus versus Plastic Strain

A decrease of Young's modulus with increasing of plastic strain is observed for the material as shown in Figure 7. Similar reduction of Young's modulus with plastic straining has been observed by Morestin and Boivin (1996). Consideration of the variation of Young's modulus vs. the plastic strain allows for a better numerical evaluation of the springback in the numerical simulations. Some studies have shown that the larger the plastic strain, the more important the difference between numerical simulations and experiments (Zang et al., 2007; Pouzols, 2010) when the Young's modulus variation is not considered.

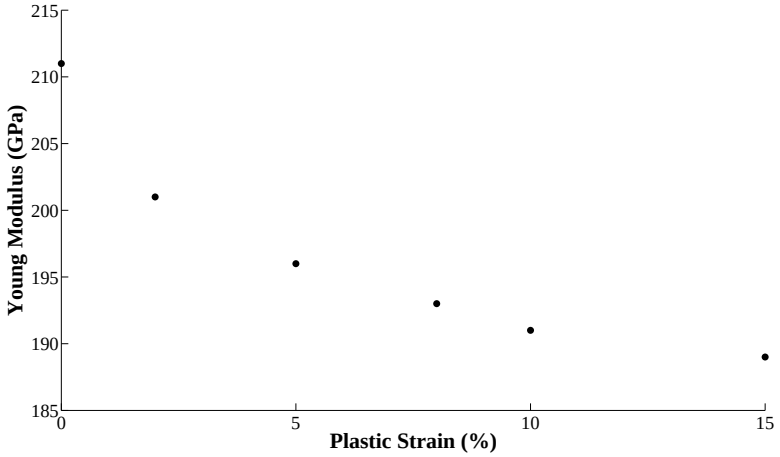

Figure 7. Young's modulus vs. plastic strain for various tensile tests on C68 steel sheets

4 Plastic Behaviour

4.1 Experimental Design

The tensile test procedure consists in heating up the sample to a given temperature. Then, the sample is deformed according to the testing parameters, at constant strain rate. The tensile machine allows us to perform tests with strain rates ranging from $10^{-3}\ /s$ to $10^{-1}\ /s$. In the present study, experiments have been achieved at strain rates equal to $10^{-3}\ /s$, $10^{-2}\ /s$ and $10^{-1}\ /s$.

The temperature sensitivity is determined by tests carried out at different temperatures. Tests have been performed at temperatures 25°C, 175°C, 350°C, 550°C and 720°C with strain rate $10^{-1}\ /s$.

4.2 Strain Rate Sensitivity

Results reported in this section refer to the behaviour of the material in the necking area of tested samples. The equivalent stress is determined by Bridgman's method as described in the previous paragraph. Figure 8 shows the strain rate sensitivity of the C68 material.

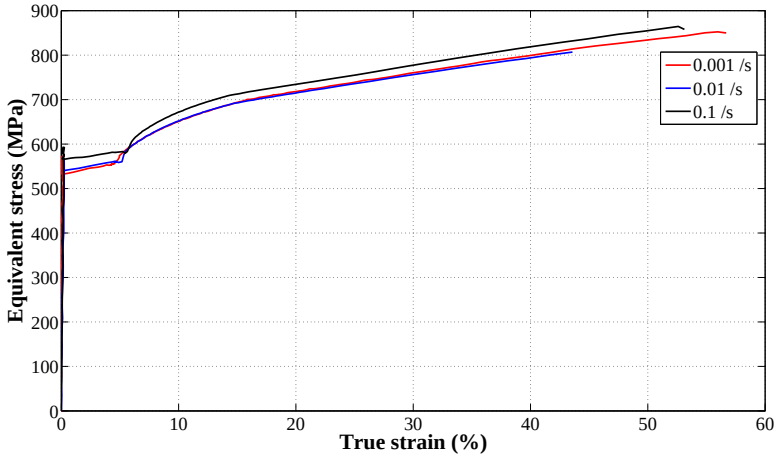

Figure 8. Experimental tensile behaviour including estimation following Bridgman's method for the C68 material at different strain rates at room temperature

The experimental behaviour at room temperature shows a Lüders' plateau. This plateau is present until the band fronts disappear in the sample heads. The analysis of the curves shows the limited influence of the strain rate.

4.3 Temperature Sensitivity

Figure 9 and Figure 10 show the temperature sensitivity of the C68 material using a virtual extensometer from the grid deformation (Figure 5) and including data from the necking area with Bridgman's method. As previously stated, results from an extensometer show the global behaviour. At higher temperatures, the onset of diffuse necking occurs earlier than at room temperature, and thus the measurements with DIC and Bridgman's methods are essential.

At 350°C, an inverse temperature sensitivity is observed. This observation characterizes the presence of dynamic strain aging in the material. That is why the necking area is outside of the surface monitored by the high-speed camera at this temperature.

Bridgman's estimation allows us to obtain equivalent stresses after the onset of the diffuse necking for the tested temperatures and strain rates.

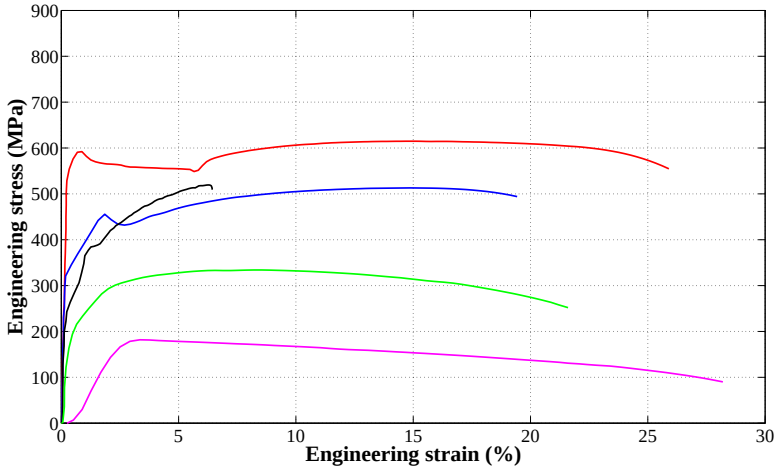

Figure 9. Experimental tensile behaviour by simulating a virtual extensometer from the grid deformation for the C68 material at different temperatures at strain rate $10^{-1}\ /s$

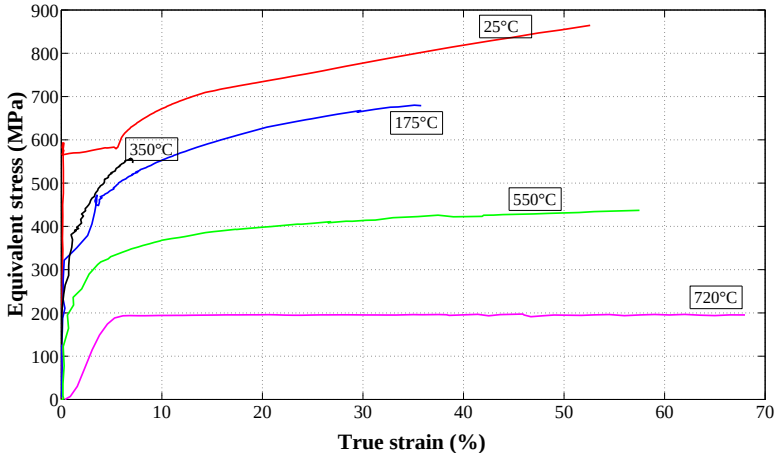

Figure 10. Experimental tensile behaviour including estimation following Bridgman's procedure for the C68 material at different temperatures at strain rate $10^{-1}\ /s$

These first results that allow for accurate observation of Lüders bands or dynamic strain aging effects prove the pertinence of the choice of the experimental setup. Furthermore, the experiments are rapid to conduct as no heating-up time is necessary.

5 Conclusions and Prospects

Metallic materials are increasingly deformed in severe conditions in forming processes. Therefore, it is necessary to carry out relevant experiments to determine accurately the mechanical behaviour of the material at high-temperature and various strain rates.

To estimate the springback, an important phenomenon in a forming process, the characterization of the material includes an accurate determination of the Young's modulus using loading-unloading cycles. The Young's modulus is only determined for a strain rate of $10^{-3}\ /s$ at room temperature.

An experimental set-up for high-temperature tensile testing is proposed in this paper. This set-up includes an induction system to heat the sample, controlled by a pyrometer. The full strain field is measured by the digital image correlation method. When the necking occurs, the stress distribution across the section is estimated by Bridgman's method.

Such equipment allows a characterization of the C68 steel which, despite a large utilization in industry, is not reported in today's available bibliography. The analysis of the first results shows a clear sensitivity to the temperature. Strain rate effects should be studied at higher strain rates and elevated temperatures because the rate sensitivity in the available range is not obvious. Other devices such as Hopkinson bars could be used. Further experimental plan will investigate the interaction effect of temperature and strain rate on the C68 steel. Full characterization will provide a database for further modeling and simulation.

References

Bridgman, P.: *Studies in Large Plastic Flow and Fracture*. McGraw-Hill (1952).

Le Roy, G.; Embury, J.; Edwards, G.; Ashby, M.: A model of ductile fracture based on the nucleation and growth of voids. *Acta Metallurgica*, 29, (1981), 1509–1522.

Liu, J.; Lyons, J.; Sutton, M.; Reynolds, A.: Experimental characterization of crack tip deformation fields in alloy 718 at high temperatures. *Journal of Engineering Materials and Technology*, 120, (1998a), 71–78.

Liu, J.; Sutton, M.; Lyons, J.; Deng, X.: Experimental investigation of near crack tip creep deformation in alloy 800 at 650c. *International Journal of Fracture*, 91, (1998b), 233–268.

Lyons, J.; Liu, J.; Sutton, M.: High-temperature deformation measurement using digital image correlation. *Experimental Mechanics*, 36, (1996), 64–70.

Morestin, F.; Boivin, M.: On the necessity of taking into account the variation in the young modulus with plastic strain in elastic-plastic software. *Nuclear Engineering and Design*, 162, (1996), 107–116.

Pan, B.; Wu, D.; Xia, Y.: High-temperature deformation field measurement by combining transient aerodynamic heating simulation system and reliability-guided digital image correlation. *Optics and Lasers in Engineering*, 48, (2010), 841–848.

Pouzols, V.: *Optimisation d'opérations industrielles de pliage par la méthode des éléments finis*. Ph.D. thesis, Université de Savoie (2010).

Raujol-Veillé, J.; Toussaint, F.; Tabourot, L.; Vautrot, M.; Balland, P.: Fe simulation of a thin-wall short-tube forming process. In: *ESAFORM* (2011).

Temimi-Maaref, N.: *Comportement thermo-mcanique et rupture de polypropylnes. Etude exprimentale et modlisation.*. Ph.D. thesis, Ecole des Mines de Paris (2006).

Vacher, P.; Dumoulin, S.; Morestin, F.; Mguil-Touchal, S.: Bidimentional strain measurement using digital images. *Proceedings of the Institution of Mechanical Engineers, Part C: Journal of Mechanical Engineering Science*, 213(8), (1999), 811–817.

Zang, S.; Liang, J.; Guo, C.: A constitutive model for spring-back prediction in which the change of young modulus with plastic deformation is considered. *International Journal of Machine Tools & Manufacture*, 47, (2007), 1791–1797.

Zhang, Z. L.; Hauge, W.; Ødegård, J.; Thaulow, C.: Determining material true stress-strain curve from tensile specimens with rectangular cross-section. *International Journal of Solids and Structures*, 36, (1999), 3497–3516.

Addresses: Mathieu Vautrot, Pascale Balland, Laurent Tabourot, Jonathan Raujol-Veillé, Franck Toussaint, Laboratoire SYMME, Université de Savoie, Annecy le Vieux.
Odd Sture Hopperstad, SIMLab, Norwegian University of Science and Technology, Trondheim.
email:
mathieu.vautrot@univ-savoie.fr; pascale.balland@univ-savoie.fr;
odd.hopperstad@ntnu.no; laurent.tabourot@univ-savoie.fr;
jonathan.raujol-veille@univ-savoie.fr; franck.toussaint@univ-savoie.fr